




Article

Effect of pH on Electrochemical Impedance Response of Tethered Bilayer Lipid Membranes: Implications for Quantitative Biosensing

Arun Prabha Shivabalan ¹, Filipas Ambrulevicius ¹, Martynas Talaikis ¹, Vaidas Pudzaitis ², Gediminas Niaura ^{1,2} and Gintaras Valincius ^{1,*}

¹ Department of Bioelectrochemistry and Biospectroscopy, Life Sciences Center, Vilnius University, 10257 Vilnius, Lithuania; shivabalan.arun@bchi.stud.vu.lt (A.P.S.); filipas.ambrulevicius@bchi.stud.vu.lt (F.A.); martynas.talaikis@gmc.vu.lt (M.T.); gediminas.niaura@ftmc.lt (G.N.)

² Department of Organic Chemistry, Center for Physical Sciences and Technology (FTMC), Sauletekio av. 3, 10257 Vilnius, Lithuania; vaidas.pudzaitis@ftmc.lt

* Correspondence: gintaras.valincius@gmc.vu.lt

Abstract: Tethered bilayer lipid membranes (tBLMs) are increasingly used in biosensor applications where electrochemical impedance spectroscopy (EIS) is the method of choice for amplifying and recording the activity of membrane-damaging agents such as pore-forming toxins or disrupting peptides. While the activity of these biological agents may depend on the pH of the analytes, there is increasing evidence that the sensitivity of tethered bilayer sensors depends on the pH of the solutions. In our study, we addressed the question of what are the fundamental reasons for the variability of the EIS signal of the tBLMs with pH. We designed an experiment to compare the EIS response of tBLMs with natural membrane defects and two different membrane disruptors: vaginolysin and melittin. Our experimental design ensured that the same amount of protein and peptide was present in the tBLMs, while the pH was varied by replacing the buffers with different pH values. Using a recently developed EIS data analysis algorithm from our research group, we were able to demonstrate that, in contrast to previous literature which relates the variability of tBLM, EIS response to the variation in defect density, the main reason for the observed variability in EIS response is the change in the sub-membrane properties of tBLMs with pH. Using surface-enhanced infrared absorption spectroscopy (SEIRAS), we have shown that pH changes from neutral to slightly acidic leads to an expulsion of water, presumably bound to ions, from the sub-membrane reservoir, resulting in a marked decrease in the carrier concentration and specific conductance of the sub-membrane reservoir. Such a decrease is recorded by the EIS as a decrease in the conductance of the tBLM complex and affects the sensitivity of a biosensor. Our data provide important evidence of pH-sensitive effects that should be considered in both the development and operation of biosensors.

Keywords: tethered bilayer lipid membranes; EIS; pore-forming toxins; vaginolysin; melittin; SEIRAS



Citation: Shivabalan, A.P.; Ambrulevicius, F.; Talaikis, M.; Pudzaitis, V.; Niaura, G.; Valincius, G. Effect of pH on Electrochemical Impedance Response of Tethered Bilayer Lipid Membranes: Implications for Quantitative Biosensing. *Chemosensors* **2023**, *11*, 450. <https://doi.org/10.3390/chemosensors11080450>

Academic Editor: Gyöző G. Láng

Received: 16 April 2023

Revised: 4 August 2023

Accepted: 7 August 2023

Published: 11 August 2023



Copyright: © 2023 by the authors. Licensee MDPI, Basel, Switzerland. This article is an open access article distributed under the terms and conditions of the Creative Commons Attribution (CC BY) license (<https://creativecommons.org/licenses/by/4.0/>).

1. Introduction

Phospholipids are the major component of the plasma membrane of eukaryotic cells. The plasma membrane not only acts as a physical barrier but also helps to regulate the movement of various ions and molecules into and out of the cell [1]. The plasma membrane, which has both a hydrophobic core and hydrophilic leaflets, acts in a capacitive manner by interacting with charged ions on the hydrophilic outer leaflets and being electrically insulating in its hydrophobic core [2]. Understanding the electrochemical interactions of this system under in vivo conditions can be very challenging, so there is a need for simpler model systems to elucidate the interactions of lipid membranes with their surrounding ionic environment. Some of the common model systems used for this purpose include

black lipid membranes, planar lipid membranes and tethered bilayer lipid membranes (tBLMs) [3].

Tethered bilayer lipid membranes (tBLMs) (Figure 1) are one of the most robust tools for understanding the electrochemical properties of the lipids that make up the lipid bilayer [4]. tBLMs are lipid bilayer membranes that are anchored to a solid support by anchoring molecules. The preparation of tBLMs is a two-step process. In the first step, the anchoring molecules are self-assembled on the solid support together with a back-filling molecule, forming the self-assembled monolayer (SAM). Lipid vesicles of the desired composition are then added to this SAM to form tBLMs. This tethering architecture facilitates lateral diffusion of lipids on the membrane [5] and formation of a liquid-filled submembrane ionic reservoir between the lipid bilayer and the solid support. The thickness of this submembrane has been calculated to be 1–2 nm [4,6]. tBLMs form electrically insulating membranes [7]. The electrochemical properties of tBLMs can be measured using electrochemical impedance spectroscopy (EIS). EIS has been the popular technique of choice used to test tBLM formation from different lipid compositions mimicking bacterial membrane [8], yeast cell membrane [9] and mammalian cell membrane [10]. EIS based tBLM studies are also employed to understand the interaction of lipid bilayer with membrane proteins [11–14].

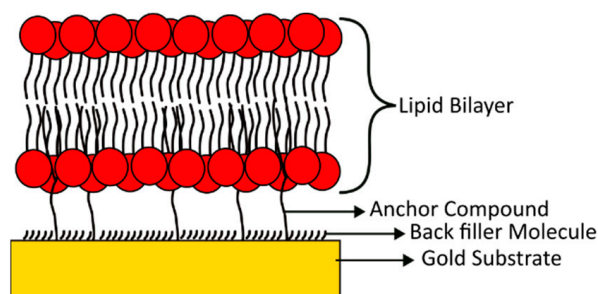


Figure 1. Cartoon of tBLM architecture.

tBLMs have been found to have stable insulating membranes for longer durations. The study by Vockenroth [15] shows that tBLMs were observed to have stable electrically insulating membranes for as long as three months. Due to this stable nature, tBLMs have potential applications as biosensors. The study by Tun and Jenkins [16] described the concept of tBLMs as a sensing platform for the detection of virulent pore-forming toxins from cultured *Staphylococcus aureus*. This concept of tBLM-based biosensors has attracted interest, particularly for its potential applications in pharmacology and clinical diagnostics. One of the most recent developments in this field is a tBLM-based nanoelectronic biosensor [17], which demonstrated real-time single ion channel recording of alamethicin incorporated into tBLMs and synthesized on a single-walled carbon nanotube nanoelectronic device. Therefore, there is a great need to understand the fundamental properties of tBLMs and their response characteristics in order to develop a tBLM-based biosensor. One of the parameters that needs to be controlled in the design and application of tBLM-based biosensors is the pH environment surrounding the tBLM. Initial investigation by Krishna et al. [18] reported that the reservoir resistivity (ϵ) of the submembrane region has a significant contribution to the overall conductivity of tBLM. Later, the study by Valincius et al. [19] presented a rigorous mathematical analysis of the effect of the submembrane region on the electrochemical response of tBLMs. The studies by Cranfield et al. [20] and Silin [21] have demonstrated the changes in the conductivity of tBLMs as a function of pH and also predicted the potential interactions of lipid head groups with ionic and non-ionic species in the surrounding solution. Both authors hypothesize that the pH-induced changes in tBLM conductivity are related to the structural rearrangement of the lipid bilayer with pH. In these studies, the properties of the submembrane region and their variation were not considered as a primary cause of the observed conductivity changes of tBLMs. On the other hand, there is increasing evidence that the conductivity

of sparsely bound tBLMs is primarily determined not by the conductivity of a single defect, but rather by the conductivity of the point defect surrounding the submembrane space [19]. We hypothesize that the observed pH effects may be primarily related to the modulation of sub-membrane conductance rather than the variation of defect densities as suggested [20,21]. If this hypothesis is correct, the pH-dependent properties of tBLMs must be taken into account in order to allow a precise quantitative analysis.

The aim of the current study is to investigate the pH dependence of the tBLM EIS response, which can be used as a readout in tBLM-based biosensors. In order to evaluate the effect of phospholipid composition on pH-driven conductivity changes, we have chosen several cholesterol-containing tBLMs, specifically 1,2-dioleoyl-sn-glycero-3-phosphatidylcholine (DOPC)/cholesterol (Chol) 50:50 (mol%), 70:30 (mol%) and natural lipid composition from total lipid extract (TLE) of a porcine brain. The two former compositions are neutral at pH 7 and slightly positively charged at pH 4 [22]. The latter composition, namely TLE, contains charged lipid species such as phosphatidylserine (PS) and phosphatidylinositol (PI) (URL: <https://avantilipids.com/product/131101>, accessed on 25 February 2023). All three membrane compositions were populated with natural (spontaneously formed) defects, and we also artificially populated tBLMs with either a large protein pore formed by the cholesterol-dependent cytolysin (CDC)-vaginolysin (VLY) or the melittin (MEL) peptide from *Apis mellifera* bee venom. In all three cases, the nature of the defects was different. While naturally occurring defects can be arbitrary in shape and are primarily related to mispackaging and punctate or lateral defects in the solid substrate, CDC forms large circular defects up to 50 nm in diameter, while MEL affects membranes in one of two ways. At lower concentrations, MEL binds parallel to the outer leaflet of the membrane; this orientation of MEL is reported to have a protective effect on the membrane [23]. Alternatively, it inserts perpendicular to the membrane, forming transmembrane pores at higher concentrations [24]. In our case, due to the relatively high concentration, the most likely form of MEL defects are relatively narrow transmembrane pores, approximately 4.4 nm in size [25]. To analyze the response of the electrical properties of tBLMs to pH change, we used the recently developed EIS data analysis technique, which allows to estimate both the average density of conductive defects and the lateral density distribution function [26]. The main result of the current study may help to understand the nature and mechanism of tBLMs response to electrochemical perturbation, which is of utmost importance for the development of smart biosensor devices that can operate in different variable pH environments.

2. Materials and Methods

2.1. tBLM Preparation

For EIS, glass substrates were coated with Cr underlayer (~10 nm) and Au (~100 nm) using magnetron sputtering system (Lesker PVD 75, St. Leonards-on-Sea, UK). Then, the substrates were incubated for 12 h at room temperature in an ethanol solution containing 0.05 mM of thiols, anchor thiol WC14 (20-tetradecyloxy-3,6,9,12,15,18,22-heptaaxahexatricontane-1-thiol; synthesized in-house) and β -mercaptoethanol (ME; Sigma-Aldrich, St. Louis, MO, USA) at 35:65 mol% ratio. Post incubation, substrates were rinsed with ethanol, dried under a nitrogen stream, and immediately assembled into an electrochemical cell, where they functioned as working electrodes. The cell consisted of 12 independent 250 μ L volume wells, with surface area of 0.16 cm² each. The tBLMs were formed on the anchoring WC14/ME monolayers by multilamellar vesicles (MLV) fusion in individual wells. Briefly, to form MLVs, the stock solution of TLE in chloroform (Avanti polar lipids, Birmingham, AL, USA) (10 mM, 0.1 mL) was added to a vial and evaporated under gentle nitrogen stream to form a thin lipid film. The film was rehydrated with a phosphate buffer solution (PBS) (NaCl 137 mM, KCl 27 mM, Na₂HPO₄ 10 mM, KH₂PO₄ 1.8 mM, pH 4.4) to a total of 1 mM concentration and mixed until it became homogeneous and milky. Similarly, the 50:50 and 70:30 mol% MLV solutions of DOPC:Chol (Avanti polar lipids, Birmingham, AL, USA) were prepared as well. The freshly prepared MLV solution was added into the

EIS wells (100 μL per well), incubated for 30 min, and thoroughly rinsed with 10 mL of PBS pH 4.4. The initial EIS response was measured after 15 min equilibration with PBS pH 4.4, followed by pH exchange to 7.1 and EIS measurement. To assess the pH effects on tBLMs affected with pore-forming toxins, either 1.5 nM of VLY (expressed and purified as described earlier [27]) or 1 μM of MEL (Sigma-Aldrich, St. Louis, MO, USA) was incubated for 30 min along with tBLMs maintained at pH 7.1. To remove excess of non-reconstituted toxins, wells were rinsed with toxin-free pH 7.1 PBS buffer and subjected to EIS. After that, the pH was shifted to 4.4, allowing it to equilibrate for 15 min, and the EIS was repeated. pH was exchanged twice on toxin-reconstituted tBLMs to quantify the change in the frequency minimum (f_{min}) position in log scale.

2.2. EIS Measurements

EIS was measured using a Zennium electrochemical workstation (Zahner, Kronach, Germany). The impedance spectra were obtained in potentiostatic mode with 10 mV alternating current at 0 V bias against the reference electrode in aerated solutions. The frequency range was 0.1 Hz to 100 kHz, with 10 logarithmically distributed measuring points per decade. A saturated silver–silver chloride (Ag/AgCl/NaCl (aq. sat.)) microelectrode (M-401F, Microelectrodes, Bedford, NH, USA) was used as the reference (+196 mV vs. SHE), and the auxiliary electrode was a platinum wire (99.99% purity, Aldrich; diameter = 0.25 mm) wound around the tube of the reference electrode.

2.3. Calculation of Defect Density Distribution and Sub Membrane Capacitance

The electrochemical impedance of a tethered lipid bilayer membrane can be understood in terms of an equivalent circuit (Figure 2), where Z_{mem} is a serial combination of Helmholtz capacitance and lipid bilayer capacitance, Z_{def} is the resistance of a conducting defect and Z_{sub} is the impedance of the sub-membrane reservoir. Around the characteristic frequency f_{min} , the dominant contribution comes from Z_{sub} . For a given sub membrane resistance (ρ_{sub}), Z_{sub} is a measure of how far apart the defects are [19]. Therefore, the position of f_{min} can be used to estimate the surface density of conductive defects by using the empirical relationship Equation 34 in [19].

$$Z_{\text{mem}} = 1/j2\pi f[(\delta^2 - r^2)(C_m^{-1} + C_H^{-1})^{-1} + \pi r_0^2 C_H], \quad (1)$$

$$Z_{\text{sub}} = 2\pi\Lambda \frac{H_1^2(L\Lambda)H_1^1(\Lambda) - H_1^1(L\Lambda)H_1^2(\Lambda)}{H_1^2(L\Lambda)H_0^1(\Lambda) - H_1^1(L\Lambda)H_0^2(\Lambda)}, \quad (2)$$

where r_0 —radius of the conductive pore in the bilayer and δ —distance to the boundary of the region which can also be expressed as defect density $N_{\text{def}} = 1/\pi\delta^2$, C_m —capacitance of the bilayer, C_H —capacitance of the Helmholtz layer at the substrate, $L = \delta/r_0$, ρ_{sub} and $\Lambda = (1 - j)r_0\sqrt{2\pi f/2k}$, $k = d_{\text{sub}}/(\rho_{\text{sub}}C_H)$. Around characteristic frequency f_{min} , dominant contribution to overall impedance comes from Z_{sub} . This impedance is characterized by L and Λ , as shown in Equation (2). Out of all the physical parameters that are inside L and Λ , δ and ρ_{sub} are the ones we address most carefully in the scope of this work. Turns out that by fitting EIS spectra, only ratio of $d_{\text{sub}}\delta/\rho_{\text{sub}}$ can be calculated. However, estimates for ρ_{sub} [28] and d_{sub} [6] values are available in the literature. Given certain values for ρ_{sub} and d_{sub} , Z_{sub} in a vicinity of f_{min} is dependent mostly on δ or N_{def} [19]. Therefore, position of f_{min} can be used to estimate surface density of conductive defects by using empirical relationship from Equation (3) [19].

$$\lg(N_{\text{def}}) \approx 0.93\lg(f_{\text{min}}) - \lg(k) - \lg(r_0) - \text{const}, \quad (3)$$

where k is a time constant $\frac{d_{\text{sub}}}{\rho_{\text{sub}}C_H}$, r_0 —defect radius.

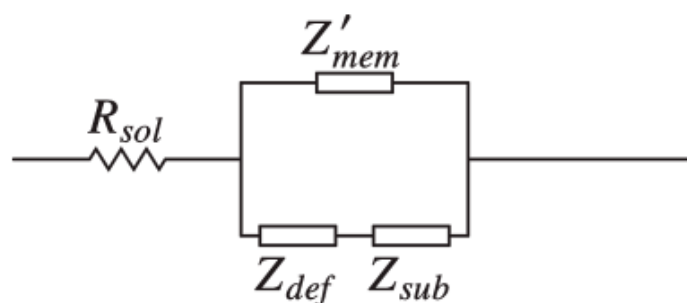


Figure 2. Equivalent Circuit.

Other theoretical aspects of electrochemical impedance spectroscopy of non-homogeneous tethered lipid bilayers were studied extensively [26,29]. The main conclusions from these studies are that EIS method is sensitive not only to defect density but also to lateral distribution of conductive defects. Main caveat of the method is that average defect density is correlated with ρ_{sub} used in calculations. Previous study [28] has addressed this issue and estimated ρ_{sub} to be around $\sim 10^4$ Ohm \cdot cm to 10^5 Ohm \cdot cm. Since, current in two regions with local density N_{defi} and N_{defj} flow parallel, admittances of these regions can be added. If one would calculate area normalized admittance Equations (1) and (2) for each region, they would need to be weighted by their relative area P_i and P_j , respectively. If there are more regions with different defect densities, the admittance of this heterogeneous tBLM Equation (4) can be written in terms of admittance integral over different defect densities [26].

$$Y_{hetero} = \int_0^{\infty} P(N_{def}) Y(N_{def}) dN_{def}, \quad (4)$$

where Y_{hetero} —is impedance of heterogeneous tBLM, N_{def} —defect density, $Y(N_{def})$ —local admittance also dependent on other parameters (for more details please see [19,26,29]) and $P(N_{def})$ is a probability density function. $P(N_{def})$ for randomly distributed defect is well modelled by gamma and/or log-normal distribution, but for experimental cases, it is usually different due to clustering of defects induced by pore-forming toxins. $P(N_{def})$ can be calculated by solving regularized and discretized form of Equation (4) as described in [26]. As can be seen from Equation (4), information about lateral distribution of defects is encoded in EIS spectra. Previous analysis of clustering impact on appearance of EIS spectra revealed that clustering results in a widening of the phase minima in a bode phase plot, as well as characteristic point $\arg Y_{min}$ shifts up and towards lower frequencies [29]. At the same time, step-like feature on the impedance magnitude vs. frequency plot becomes less flat and spreads over a wider frequency range. For a system with known size of conductive defects clustering may be estimated by using zeta parameter, as described in [29], as long as clustering does not result in multiple $\arg Y_{min}$ which can be seen in case of extreme clustering.

2.4. Surface-Enhanced Infrared Absorption Spectroscopy (SEIRAS) Measurement

The SEIRAS substrate preparation is as follows: the surface of polished face-angled Si crystal was chemically reduced with aqueous HF (2 wt%) solution and then coated with Au by covering it with plating mixture for 4 min at room temperature. Then the fresh Au film was removed by concentrated aqua regia and coated with Au for a second time, in order to increase mechanical resistance of the gold layer [30]. Au plating solution comprised (1) salt solution (0.15 M Na_2SO_3 ; 0.05 M $\text{Na}_2\text{S}_2\text{O}_3$; and 0.05 M NH_4Cl), (2) NH_4F (20 wt%), (3) HF (2 wt%) and (4) NaAuCl_4 (0.03 M) in equal volumes. Gold-coated Si was mounted into VeeMax III accessory with Jackfish cell J1F (Pike Technologies, Fitchburg, WI, USA) and additionally cleaned and activated by electro polishing procedure in N_2 -purged pH 5.8 sodium acetate solution (0.1 M). Cyclic voltammetry (CV) scans were performed on PGSTAT101 potentiostat (Metrohm, Riverview, FL, USA) with initial and stopping potential set at ± 200 mV of the open circuit potential (OCP) and scanning rate of 20 mV/s. The

upper potential limit was increased by 100 mV after each of three full cycles until the gold oxidation was reached near 1.0 V.

SEIRAS measurements were carried out using Vertex 80 v (Bruker, Mannheim, Germany) spectrometer equipped with liquid nitrogen-cooled narrow-band LN-MCT (HgCdTe) detector. The spectral resolution was set to 4 cm^{-1} , the aperture to 2 mm, 50 sample scans and 100 background scans were co-added. The incident angle for VeeMax III accessory was set to 63 degrees. Spectrometer was purged with dry air overnight.

2.5. Formation of SAM and tBLM for SEIRAS Measurement

Gold substrates were incubated in a mixed solution of 35% molar ratio of WC14 and 65% molar ratio of β -mercaptoethanol. These compounds were dissolved in ethanol in their respective molar ratios. Incubation was carried out for 12 h at room temperature. Post incubation, the substrates were rinsed with ethanol and dried under a stream of nitrogen gas and immediately used for experiments. tBLM formation was prepared using DOPC/Chol 70:30 compositions similar to the EIS technique. For pH shift experiment, 0.05 M phosphate solutions with 0.1 M Na_2SO_4 and pH values of 4.5 and 7.3 were used.

3. Results and Discussion

3.1. EIS and Data Analysis

In this work, the EIS technique is used to assess the function, density and structural arrangement of defects in tBLMs. While all types of data representation are suitable for EIS analysis, the Bode plots are used to track the properties of tBLMs in this work. One of the main features used in this work is the position of the minimum of the impedance admittance in the frequency domain. The highly electrically insulating membranes with few defects show the f_{\min} in the lower frequency range ($<1\text{ Hz}$), in contrast to the highly defective protein pore-populated membranes, where the f_{\min} is shifted to higher frequency ranges ($>100\text{ Hz}$) in the Bode phase plots. It is worth noting that the admittance phase minimum at f_{\min} corresponds to the step-like feature in the admittance magnitude versus frequency plots. In the current study, the admittance phase plots were used to assess the pH-induced effects on the EIS response.

tBLMs are highly asymmetric. The distal leaflet of tethered lipid bilayers is bathed by the bulk electrolyte, while the proximal side is in contact with the highly confined 1–2 nm ionic reservoir, which in addition to water molecules also contains PEG chains of molecular tethers (concentration up to 40% as indicated by neutron scattering experiments) [6]. Previous estimates indicate that the resistance of the sub-membrane reservoir is very different from that of the bulk electrolyte [28]. In such a confined environment, the molecular interactions between the components of the sub-membrane and the head groups of the bilayer from one side, and the Helmholtz layer at the metal/reservoir interface from the other side may exhibit structural ordering/disordering effects, which in turn should be reflected in the electrical properties of the sub-membrane reservoir. For example, it has been found that due to the partial loss of the hydration shell and ion–ion correlation in confined aqueous electrolytes, the mobility of the ions is significantly reduced [31]. In addition, the reduction of the dielectric constant in the sub-membrane will immediately trigger a reduction in ion concentration due to the increased electrochemical potential (free energy of an ion) of an ion. All of these effects are expected to result in changes in the electrical properties of the sub-membrane as well as changes in the measured EIS.

How much can the sub-membrane resistance contribute to the measured EIS? According to [19], the answer to this question depends on the ratio between the impedance of an ion channel (defect) and the impedance of the sub-membrane. Figure 3 shows these ratios for several ion channels with different conductivities from 10 pS to 500 pS. Since the impedance of the sub-membrane reservoir is determined by the defect density [19], the ratio $\sigma_{\text{def}}/Y_{\text{sub}}$ also depends on N_{def} . Y_{sub} also depends on the physical parameters of the sub-membrane, such as the specific resistance. The latter can be estimated from AFM measurements and was found to be $\rho_{\text{sub}} = 10^{4.5}\text{ Ohms} \cdot \text{cm}$ [28].

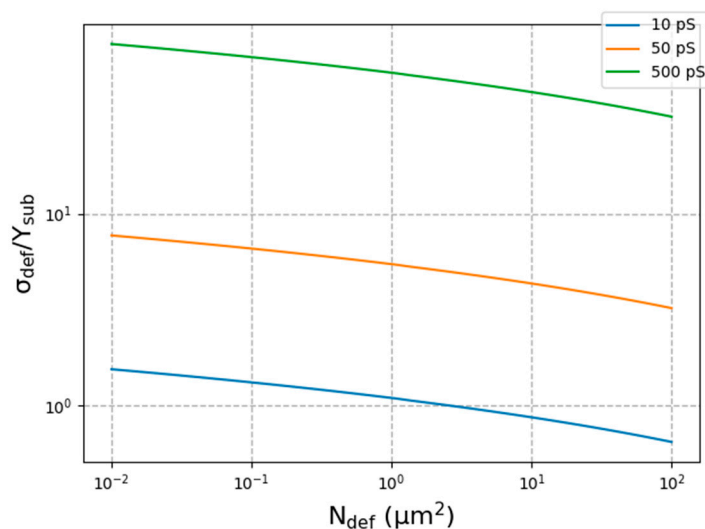


Figure 3. Plot showing the ratio of defect conductance and conductance of sub membrane reservoir as a function of defect density. Conductance of sub membrane reservoir is taken to be absolute conductance at f_{\min} . Parameters used for modelling $C_m = 0.6 \mu\text{F}/\text{cm}^2$, $C_H = 10 \mu\text{F}/\text{cm}$, $\rho_{sub} = 10^{4.5}$ and σ_{def} values are indicated in the plot.

The data in Figure 3 were calculated using the analytical solution for the sub-membrane conductance in the case of a homogeneous (hexagonal array) distribution of defects [19]. It is obvious that in the tBLMs used in the current work, the sub-membrane reservoir is the major contributor to the measured EIS admittance unless the channel conductance is below 50 pS. Especially in the current study, the conductance of the inserted MEL channel should be in the range of 50 to 300 pS, so it is quite safe to assume that the major contribution to EIS is determined by the properties of the sub-membrane reservoir, but not by the channel itself. This means that for the observer, any change in the sub-membrane properties, such as the specific resistance, can result in a corresponding change in the admittance spectra. Specifically, the increase in resistivity is seen as an increase in impedance and a decrease in admittance of the tBLMs. It is also true that the corresponding variation in defect density will result in exactly the same changes. For example, a decrease in defect density will result in an increase in the impedance of the tBLMs. Thus, a priori, if some external stimuli affect the properties of tBLMs and trigger changes in the measured impedance, the EIS data cannot give any indication as to what is the underlying cause of the observed variation: the change in defect density or the change in electrical parameters of the sub-membrane reservoir.

In this work, in order to answer the question of what is the primary cause of the observed variations in the EIS signal induced by the pH change, we started with the following three hypotheses, all of which could be behind the observed effect:

1. The pH does not change the defect density (N_{def}) and the probability density function $P(N_{def})$ for randomly distributed defects, thus the pH-induced change of the position f_{\min} on EIS phase plot originates from the variation of sub membrane resistance ρ_{sub} , (constant N_{def}).
2. The change in sub membrane resistance ($\Delta\rho_{sub}$) is negligible, therefore, f_{\min} varies because of changes in N_{def} and $P(N_{def})$, (constant $\Delta\rho_{sub}$).
3. The N_{def} does not change while $P(N_{def})$ can vary freely, therefore, the position of f_{\min} is affected by variation of $\Delta\rho_{sub}$ and to some extent by later redistribution of defects induced by pH variation (constant N_{def} , variable $P(N_{def})$ and ρ_{sub}).

To fit the experimental data to a model, we used the methodology described in [26]. For the first hypothesis, we assumed that a single (joint) distribution function for the spectra at pH 7.1 and pH 4.4 is the same, while for pH 7.1 solutions the value of $\rho_{sub} = 10^{4.5}$ was

assigned following previous estimates [28], while for pH 4.4 this parameter was fitted to account for the shift of f_{\min} towards lower frequencies.

For the second hypothesis, the value $\rho_{sub} = 10^{4.5}$ was used for both pH 7.1 and pH 4.4, while the average defect densities and their distribution function were allowed to vary freely during fitting. For the third hypothesis, the average defect density was assumed to be the same at pH 7.1 and pH 4.4, but the distribution function was allowed to vary, and similarly to the first hypothesis, ρ_{sub} was fitted for spectra corresponding to pH 4.4 to account for the change in f_{\min} . The data fitted to a model for all three hypotheses and three lipid composition—defect type combinations are discussed below.

3.2. Pristine tBLMs with Natural Defects

The EIS plots recorded at pH 4.4 immediately after completion of fusion showed that both DOPC/Chol 50:50 and TLE formed membranes with low defect density (blue line, Figure 4A,B), as indicated by the average position of f_{\min} of -0.53 and -0.37 in log values, respectively (Table 1). The mean defect density according to the estimates in Ref. [28] is much less than $0.1 \mu\text{m}^{-2}$. The highly insulating property of the DOPC/Chol 50:50 membranes can be attributed to the presence of cholesterol [32,33] in equal molar ratios with DOPC [34]. On the other hand, membranes formed with DOPC/Chol 70:30 molar ratios were less insulating compared to their tested counterparts (blue line, Figure 4C and data in Table 1) and were measured to have an average f_{\min} value of 0.05 in log scale, which translates into a defect density of approximately 0.1 cm^{-2} .

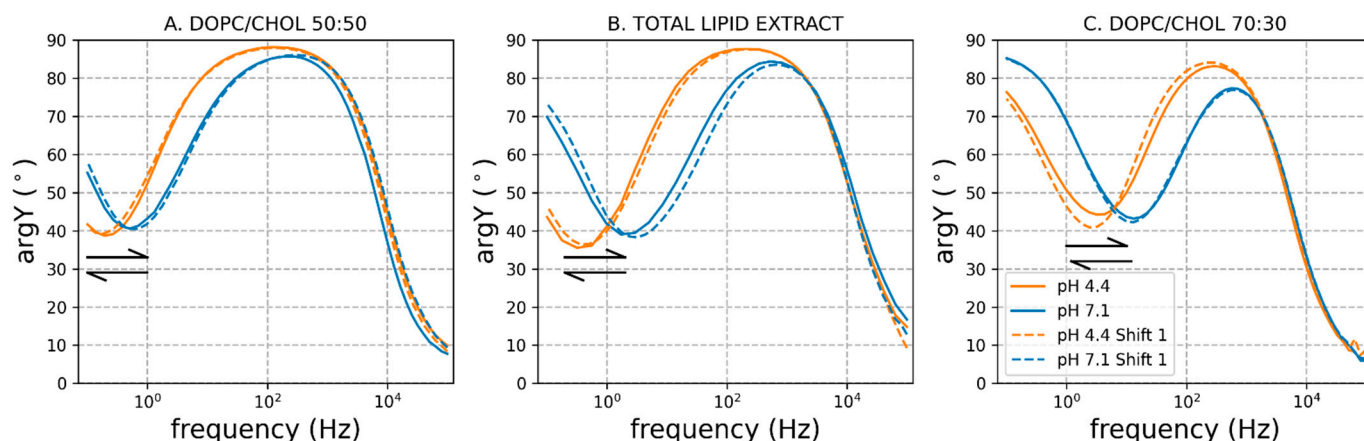


Figure 4. Representative electrochemical impedance spectra showing the phase vs. frequency plots of three different membrane compositions, DOPC/Chol 50:50, TLE and DOPC/Chol 70:30, showing pH-induced f_{\min} changes, when pH was changed from acidic (4.4) to basic (7.1). The f_{\min} tends to move towards higher frequencies as observed in all the membrane compositions (blue line, (A–C)). The f_{\min} position shifts reversibly (dashed lines, (A–C)) when changing the pH back and forth from acidic to basic on the same membranes.

Table 1. The shift $\Delta\log(f_{\min})$ triggered by the pH change from pH 4.4 to 7.1.

Membrane Composition	Average $\log(f_{\min})$ pH 4.4	Average $\log(f_{\min})$ pH 7.1	$\Delta\log(f_{\min})$ pH 4.4 \rightarrow 7.1	SD
DOPC/Chol, 50:50	-0.53	0.13	0.65	± 0.08 ($n = 6$)
TLE	-0.37	0.28	0.65	± 0.08 ($n = 5$)
DOPC/Chol, 70:30	0.05	0.70	0.65	± 0.15 ($n = 6$)

Changing the pH to 7.1 results in a shift of the f_{\min} position towards higher frequencies in all three lipid compositions (blue line, Figure 4A–C). This shift in the f_{\min} position of the tBLMs indicates an increase in the electrical conductivity of the membranes. Such an effect, an increase in membrane conductivity at higher pH, was also observed by Vitalii I.

Silin [21] and C. G. Cranfield [20] in their studies. Furthermore, the shift in f_{\min} when pH was changed from 4.4 to 7.1 resulted in a consistent shift in a logarithmic scale across all membrane compositions (Table 1). The corresponding Bode plots depicting magnitude vs. frequency dependencies are provided in the Supplemental material section (Figure S1A–C). This pattern of pH-change-induced f_{\min} shifts was consistent when the membranes were subjected to multiple pH changes between pH 4.4 and 7.1 (dashed lines, Figure 4A–C).

3.3. tBLMs Reconstituted with Defects Induced by Pore-Forming Toxins

3.3.1. VLY Reconstituted tBLMs

Pore-forming toxins and antimicrobial peptides have been used to study the structural and functional properties of tethered lipid bilayer membranes [35]. The affinity of these proteins for the lipid bilayer membranes can be used to understand the differences in the lipid composition of the membranes, thereby correlating the structural properties of the lipid bilayer membranes. CDCs are a family of pore-forming toxins that require cholesterol on the membranes for their activity, and it has been shown that the activity of this family of toxins is higher when there is a higher concentration of cholesterol on the membranes [36]. VLY is one of the CDCs used in this study to understand the effects of pH on membranes containing large pores up to 25 nm [28]. Such pores are obviously structurally different from natural defects in tBLMs. Furthermore, the density of VLY pores and the EIS response can be varied over a wide range by choosing an appropriate concentration of toxins in solutions. It has been reported that VLY is able to induce a significant shift of the f_{\min} position at a concentration of 1.5 nM.

The DOPC/Chol 50:50 tBLMs exposed to 1.5 nM VLY at pH 7.1 showed a strong response in the EIS spectra. The membrane damage by VLY pores shifted the f_{\min} position towards higher frequencies as shown in Figure 5A, blue line, and as expected from theoretical predictions [19]. The average shift in f_{\min} position due to toxin activity was found to be 2.73 ± 0.76 in the logarithmic scale (Table 2) for DOPC/Chol 50:50 membranes. DOPC/Chol 70:30 membranes containing a lower amount of cholesterol gave a significantly lower response at the same VLY concentrations. This effect is consistent with the previous study, which reported an ~three-fold reduction in the change in admittance value for membranes composed of DOPC/Chol 70:30 molar ratio compared to DOPC/Chol 50:50 membranes. Exposure of TLE tBLMs to VLY resulted in the complete destruction of the tBLMs. Therefore, we chose DOPC/Chol 50:50 compositions to test the pH effect on membranes populated with large defects of up to 25 nm radius.

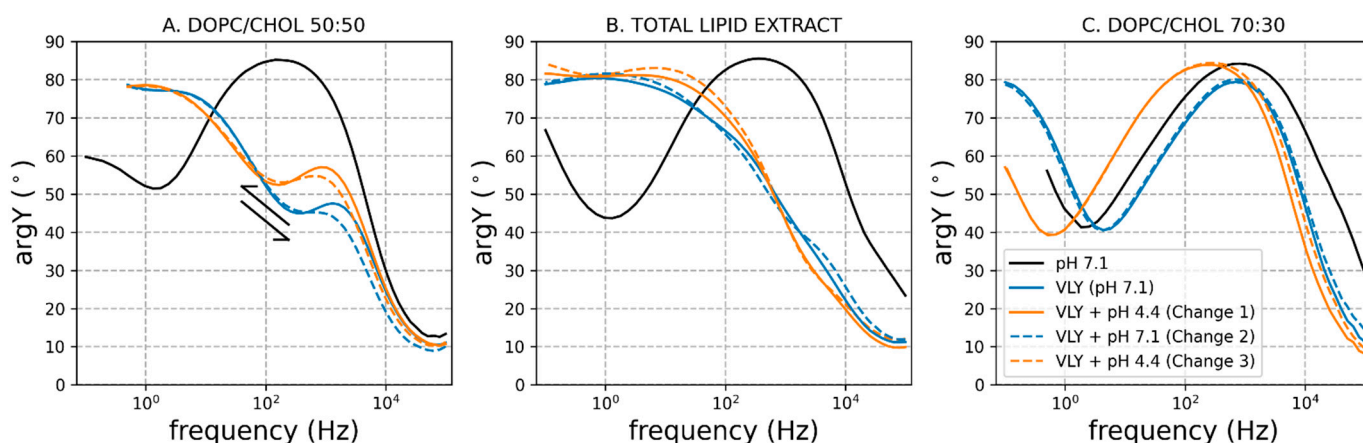


Figure 5. Representative electrochemical impedance spectra of 1.5 nM VLY affected membranes. The activity of toxin on membranes of different lipid composition can be observed by the shift in the f_{\min} towards higher frequencies (blue line, (A–C)) compared to the pristine membranes (black line, (A–C)). Reversible pH induced f_{\min} shifts observed (double sided arrows) even after the membranes were affected by VLY (dashed line, (A)).

Table 2. 1.5 nM VLY and 1 μ M MEL for 30 min at different membrane compositions in pH 7.1 buffer.

Membrane Composition	$\Delta \log(f_{\min})$ MEL	$\Delta \log(f_{\min})$ VLY
DOPC/Chol, 50:50	0.81 ± 0.61 ($n = 8$)	2.73 ± 0.76 ($n = 8$)
TLE	1.11 ± 0.31 ($n = 5$)	Completely Damaged ($n = 5$)
DOPC/Chol, 70:30	1.99 ± 0.47 ($n = 7$)	0.05 ± 0.06 ($n = 7$)

The effect of pH was investigated by changing the pH from 7.1 to 4.4. The change in the case of DOPC/Chol 50:50 tBLMs populated with VLY pores shifted the f_{\min} towards higher frequencies (blue line, Figure 5A–C), as observed for native membranes. A similar effect was observed in the case of DOPC/Chol 70:30 membranes, although the VLY-induced shift of f_{\min} was quite small (blue line, Figure 5C). The TLE membranes were completely damaged upon VLY reconstitution (blue line, Figure 5B), so the effect of pH variation on membrane conductance could not be detected. Interestingly, the observed shifts in f_{\min} in VLY-affected membranes appear quantitatively similar to the shift observed in unaffected membranes (Figure 5A,C compared to Figure 4A,C).

The hypothesis was tested by fitting the EIS data of DOPC/Chol 50:50 membranes. In DOPC/Chol 70:30 tBLMs, the VLY-induced effect was too small to be attributed to the formation of functional VLY pores, and in the case of TLE, the tBLMs were destroyed to the extent that no pH-dependent variation can be empirically recorded. Table 3 shows the fitting results for all three hypotheses (vide ultra).

Table 3. The fitting analysis of DOPC/Chol 50:50 membranes exposed for 30 min to 1.5 nM VLY solution.

Condition		pH	N_{def} (μm^{-2})	ρ ($\text{Ohm} \cdot \text{cm} \cdot 10^4$)	Ratio
constant N_{def} (Hypothesis 1)	VLY	4.4	2.34	6.21	1.96
		7.1	2.34	3.16	
	Pristine	4.4	0.12	8.05	2.54
		7.1	0.12	3.16	
constant ρ (Hypothesis 2)	VLY	4.4	1.65	3.16	1.71
		7.1	2.81	3.16	
	Pristine	4.4	0.04	3.16	1.88
		7.1	0.09	3.16	
constant N_{def} variable defect density distribution (Hypothesis 3)	VLY	4.4	2.70	5.66	1.79
		7.1	2.70	3.16	
	Pristine	4.4	0.10	6.07	1.92
		7.1	0.10	3.16	

The constant ρ_{sub} hypothesis gives the following parameters for the curves in Figure 5A: $\rho_{sub} = 3.16 \times 10^4$ ohms, with quite different defect densities. However, the ratio $N_{def}(\text{pH} = 7.1)/N_{def}(\text{pH} = 4.4)$ gives very close values for physically different systems (natural spontaneous defects and VLY pores), 1.71 and 1.88 for VLY and natural defects, respectively (Table 3). The fact that such different systems have the same ratio of pH induced change in defect density seems rather unlikely. If the membrane defect densities were changing, one would expect different defects (natural or VLY pores) to respond differently to pH variation.

The first hypothesis assumes that N_{def} is constant, but the pH change induces changes in the sub-membrane properties, specifically the resistivity. The change in resistivity should result in a proportional change in the observed EIS parameters, such as the change in EIS admittance magnitude, independent of the nature of the defects. As shown in Table 3, the ratio of $\rho_{sub}(\text{pH} = 4.4)/\rho_{sub}(\text{pH} = 7.1)$ is 1.96 and 2.54 for VLY populated and unpopulated tBLMs, respectively. The values are not exactly the same, but close.

The third hypothesis assumes constancy of global N_{def} but allows variation of the distribution of defect densities. In this case, ρ_{sub} (pH = 4.4)/ ρ_{sub} (pH = 7.1) is 1.79 and 1.92 for VLY populated and unpopulated membranes, respectively (Table 3). This suggests that pH indeed triggers the change in sub-membrane resistance, but at the same time the 2D distribution of defects may also be affected by pH variation.

3.3.2. MEL Reconstituted tBLMs

MEL is a transmembrane peptide of 26 amino acids with the sequence H2N-Gly#-Ile-Gly-Ala-Val-Leu-Lys#-Val-Leu-Thr-Thr-Gly-Leu-Pro-Ala-Leu-Ile-Ser-Trp-Ile-Lys#-Arg#-Lys#-Arg#-Gln-Gln-CONH2. The charged residues are represented by the symbol “#”. The sequence containing (Ile-Gly-Ala-Val-Leu) at the N-terminus is hydrophobic and the sequence near the C-terminus, namely Lys#-Arg#-Lys#-Arg#-Gln-Gln, is hydrophilic. A previous X-ray crystallographic study reported a highly α -helical structure in its crystalline state [25].

The current understanding of the pore formation dynamics of MEL is that these α -helical monomers, at certain concentrations, spontaneously insert into the lipid bilayer and aggregate to form a transmembrane cylindrical pore. It has been reported that MEL requires a threshold concentration of peptide–lipid ratio to form pores [37,38]. Studies show that this membrane-damaging activity of MEL is high in model membranes containing lower levels of cholesterol [39–41]. Consistent with these studies, we observed that MEL exhibited higher activity on DOPC/Chol 70:30 molar ratio membranes (blue line, Figure 6C), with an average f_{min} shift of 1.99 ± 0.47 in the logarithmic range. MEL exhibited minimal activity on the high cholesterol DOPC/Chol 50:50 membranes (Table 2). Interestingly, the significant activity of MEL was observed on TLE membranes (blue line, Figure 6B and data in Table 2) at pH 7.1, and when these membranes were subjected to pH change cycles, there was a consistent shift in the f_{min} positions of -0.53 ± 0.19 when the pH was changed from MEL activity at pH 7.1 to pH 4.4 and 0.50 ± 0.22 when the pH was changed back from 4.4 to 7.1, on the log scale. The pH shifts on DOPC/Chol 70:30 membranes after MEL activity indicate that the phenomena of f_{min} shifts induced by alternating pH is consistent and was quantified to be -0.45 ± 0.24 (Table 4) when shifting to pH 4. Four from the toxin reconstituted membranes and 0.38 ± 0.17 (Table 5) when switching back to pH 7.1 from the pH 4.4 treatment. pH shift induced change in fitted ρ_{sub} (Hypothesis 1 and 3) for pristine bilayers and MEL-damaged bilayers Tables 6 and 7 are similar. The ratios ρ_{sub} (pH = 4.4)/ ρ_{sub} (pH = 7.1) are 2.24 and 2.45 for MEL-damaged and undamaged DOPC/Chol 70:30 bilayers, respectively. A comparison of these ratios shows that ρ_{sub} shows a similar shift regardless of whether the bilayer is damaged or not. A similar observation can be made for the TLE bilayer (Table 7), where the ratios are 3.79 and 3.04 for damaged and pristine bilayers, respectively.

Table 4. The $\Delta \log f_{min}$ shifts triggered by the pH change from 7.1 to 4.4 in the presence of VLY or MEL.

Membrane Composition	$\Delta \log(f_{min})$ MEL	$\Delta \log(f_{min})$ VLY
DOPC/Chol, 50:50	-0.11 ± 0.49 ($n = 8$)	-0.33 ± 0.14 ($n = 8$)
TLE	-0.53 ± 0.19 ($n = 5$)	Completely Damaged ($n = 5$)
DOPC/Chol, 70:30	-0.45 ± 0.24 ($n = 7$)	-0.58 ± 0.21 ($n = 7$)

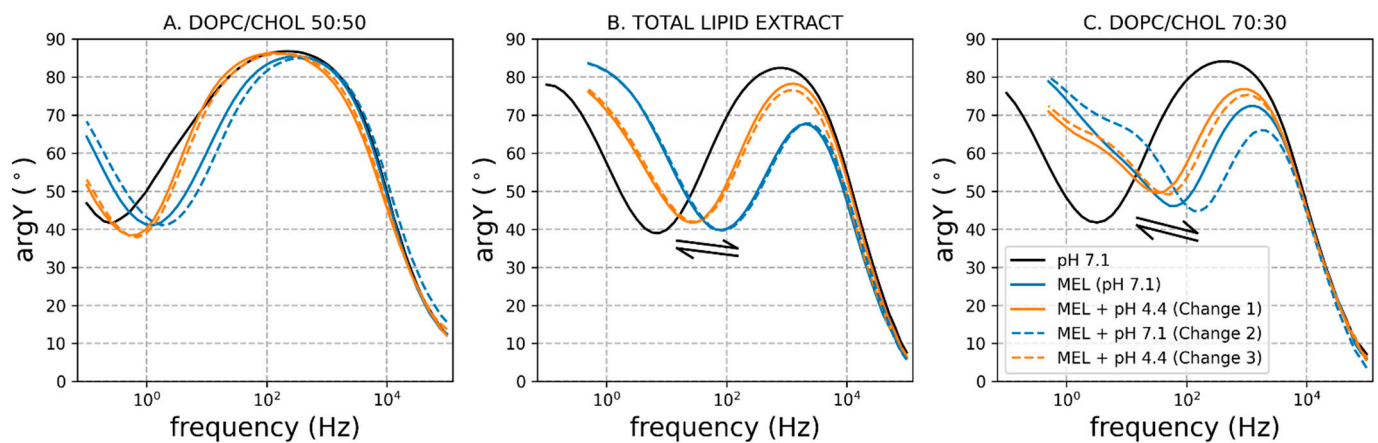


Figure 6. Representative electrochemical impedance spectra of 1 μM MEL affected membranes. The activity of toxins on membranes of different lipid compositions can be observed by the shift in the f_{\min} towards higher frequencies (blue line, (A–C)) compared to the pristine membranes (black line, (A–C)). Reversible pH-induced f_{\min} shifts were observed (double-sided arrows) even after the membranes were affected by MEL (dashed lines, (B,C)).

Table 5. The $\Delta\log f_{\min}$ shifts triggered by the pH change from 4.4 to 7.1 in the presence of VLY or MEL.

Membrane Composition	$\Delta\log(f_{\min})$ MEL	$\Delta\log(f_{\min})$ VLY
DOPC/Chol, 50:50	0.54 ± 0.08 ($n = 6$)	0.38 ± 0.10 ($n = 8$)
TLE	0.50 ± 0.22 ($n = 6$)	Completely Damaged ($n = 5$)
DOPC/Chol, 70:30	0.38 ± 0.17 ($n = 7$)	0.64 ± 0.24 ($n = 7$)

Table 6. The fitting analysis of DOPC/Chol 70:30 membranes was exposed for 30 min to 1 μM MEL solution.

Condition		pH	N_{def} (μm^{-2})	ρ ($\text{Ohm} \cdot \text{cm} \cdot 10^4$)	Ratio
constant N_{def} (Hypothesis 1)	MEL	4.4	5.60	7.62	2.24
		7.1	5.60	3.16	
	Pristine	4.4	0.09	7.74	2.45
		7.1	0.09	3.16	
constant ρ (Hypothesis 2)	MEL	4.4	5.31	3.16	2.30
		7.1	12.19	3.16	
	Pristine	4.4	0.09	3.16	2.29
		7.1	0.22	3.16	
constant N_{def} variable defect density distribution (Hypothesis 3)	MEL	4.4	12.19	6.36	2.01
		7.1	12.19	3.16	
	Pristine	4.4	0.22	7.70	2.44
		7.1	0.22	3.16	

Table 7. The fitting analysis of TLE membranes was exposed for 30 min to 1 μ M MEL solution.

Condition		pH	N_{def} (μm^{-2})	ρ ($\text{Ohm} \cdot \text{cm} \cdot 10^4$)	Ratio
constant N_{def} (Hypothesis 1)	MEL	4.4	1.12	11.98	3.79
		7.1	1.12	3.16	
	Pristine	4.4	0.04	9.61	3.04
		7.1	0.04	3.16	
constant ρ (Hypothesis 2)	MEL	4.4	0.29	3.16	3.12
		7.1	0.93	3.16	
	Pristine	4.4	0.01	3.16	2.90
		7.1	0.04	3.16	
constant N_{def} variable defect density distribution (Hypothesis 3)	MEL	4.4	0.93	12.81	4.05
		7.1	0.93	3.16	
	Pristine	4.4	0.04	12.06	3.82
		7.1	0.04	3.16	

On the other hand, the pH shift-induced changes in fitted N_{def} values (Hypothesis 2) increase by an order of magnitude for MEL-damaged bilayers (Hypothesis 2) compared to pristine bilayers. The average defect density changes from ~ 5 to ~ 12 when the pH is changed from 4.4 to 7.1 for the damaged DOPC/Chol 70:30 bilayer, while for the pristine bilayer, these values are ~ 0.1 and ~ 0.2 , respectively, as seen by the shift in the distribution functions in Figure S2C. Analogous to the DOPC/Chol 50:50 bilayer and the DOPC/Chol 50:50 bilayer damaged by VLY, to justify Hypothesis 1, it needs to be explained why the pH-induced effect is proportional to the membrane damage by the toxins.

It is noteworthy that the ratios ρ_{sub} (pH = 4.4)/ ρ_{sub} (pH = 7.1) vary much more between different bilayer compositions than between experiments with intact and damaged bilayers. This suggests that the properties of the submembrane reservoir depend on the lipid composition. Although the exact mechanism of pH-induced change is unknown, it is likely to be related to reduced mobility or concentration of mobile ions. The properties of confined electrolytes are influenced by the physicochemical properties of the confining surface and the size of the confinement. The architecture of tBLM is such that one of the confining surfaces is the proximal leaflet of a bilayer. The other surface is the double electrical layer of metal support. Different lipid compositions can alter the thickness of the bilayer, which reduces the thickness of the submembrane reservoir and different concentrations of zwitterionic or charged lipids modulate interactions with ions and the structure of the electrical double layer in the submembrane reservoir. In this context, the TLE bilayers exhibit quite different properties as can be seen from the ratio: N_{def} (pH = 7.1)/ N_{def} (pH = 4.4), which is equal to 3.12 (MEL) or 2.90 (pristine tBLM) (Table 7, Hypothesis 2); and from ρ_{sub} (pH = 4.4)/ ρ_{sub} (pH = 7.1), which is equal to 3.79 for MEL or 3.04 for native tBLM (Table 7, Hypothesis 1); 4.05 for MEL or 3.82 for native tBLM (Table 7, Hypothesis 3). The ratios for TLE are on average ~ 1 log unit higher than for DOPC/Chol 50:50 or DOPC/Chol 70:30 tBLM. This may be related to the fact that TLE contains 11% PS, 1.6% PI and 2.8 PA, which are negatively charged, in contrast to the other two bilayers studied, which contain only zwitterionic lipids and cholesterol. The increased ratio for TLE bilayers can be explained by the increased sensitivity of the properties of the submembrane reservoir to pH due to the protonation–deprotonation activities of phospholipids in TLE compositions. Interactions of lipid head groups with ionic species in the surrounding solution have been shown to influence the organization and dynamics of lipid bilayers [42–46]. Anions that bind to lipid head groups increase the area per lipid head group due to the resulting repulsive interaction. Deviation of pH from pKa of the head group makes the bilayer more disordered (defective) [42] and decreases membrane tension [43]. These effects can be responsible for more strong modulation of the sub membrane properties by the pH.

Further arguments in favor of Hypothesis 1 can be made by examining Figures S4 and S6. Fitting two separate distribution functions with the same average defect density N_{def} as

in Figure S6, results in a visibly better fit than fitting both spectra at pH 4.4 and spectra at pH 7.1 with a single distribution function in Figure S4. It can be argued that slight changes in the distributions in Figure S6C may be caused by pH-dependent reorganization of tBLM. However, all EIS spectra contain parasitic elements that are not accounted for in a model, so we argue that an approach consistent with the assumption of Hypothesis 1 results in a more physically relevant fit, as it helps to filter out frequency-dependent spectral features caused by unknown parasitic elements.

3.4. SEIRAS

SEIRAS method provides detailed molecular information on the structure of molecular assemblies on the gold surface in situ [47,48]. Characteristic of SEIRAS, the rapid plasmon-enhanced local electric field decrease along the surface normal that makes the technique particularly useful in SAM and artificial lipid-membrane studies [49–52]. Moreover, the spectral contribution from the bulk water can be almost completely cancelled by constructing a perturbation-difference spectrum (electric field, pH, etc.), which allows to probe directly the sub membrane structure of tBLM. Figure 7 shows SEIRAS spectra of tBLM in the 2830–3800 cm^{-1} range, where modes ascribed to symmetric and asymmetric methylene stretching (2856 and 2927 cm^{-1}) and asymmetric methyl stretching (2959 cm^{-1}) of alkyl chain are located. The broad negative feature around 3500 cm^{-1} is related to O–H stretching mode of water removed from the Au interface during the formation of tBLM. SEIRAS spectra of tBLM submerged in pH 4.5 and 7.3 show repeatable changes in the sub membrane water volume. As the control experiment, the tBLM was thoroughly rinsed with the phosphate solution pH 4.5, which is the same as the bathing multilayer vesicle solution, with no significant effect on the SEIRAS spectra (Figure 7). In contrast, the subsequent pH exchange to 7.3 increased the amount of interfacial water evidenced by the decrease of the negative $\nu(\text{O-H})$ mode's intensity. The process repeatability is well illustrated by pH shifting between 4.5 and 7.3 values, which resulted in a reduction of absolute integral intensity to 81–84% at pH 7.3 and an increase to 91–93% at pH 4.5 at later steps. So, we can claim that the pH exchange from 4.5 to 7.3 results in a sharp increase in water concentration in the sub membrane as evidenced by the decrease of negative $\nu(\text{O-H})$ vibrational mode intensity (Figure 7).

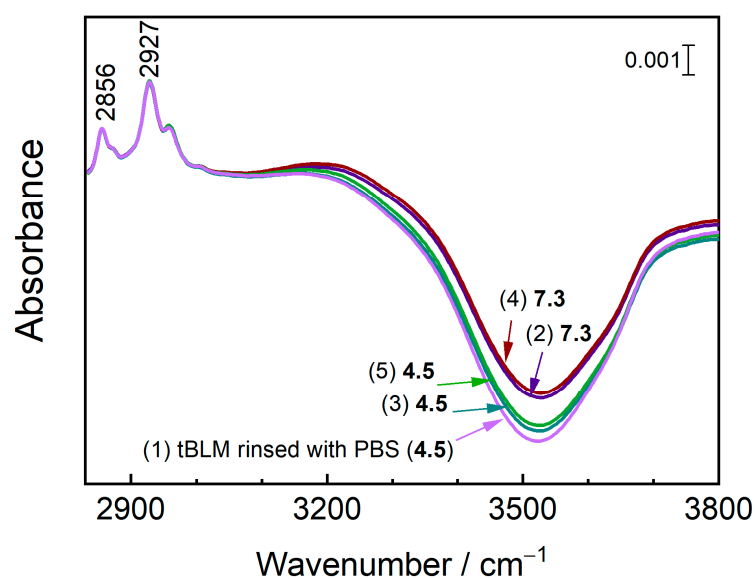


Figure 7. SEIRAS spectra in 2830–3800 cm^{-1} range of tBLM with sequential pH exchange between 4.5 and 7.3. For reference, the spectrum of pure water recorded before the adsorption of SAM was selected. Spectral intensity normalized according to the asymmetric stretching mode of methylene at 2927 cm^{-1} .

A more detailed view of the processes is seen in Figure 8, which shows SEIRAS spectra constructed by taking as-formed tBLM in pH 4.5 as a reference and tBLM subsequently exposed to pH 7.3 and then 4.5 as samples. Immediately after the pH shift to 7.3, perturbations appear in C–H and O–H stretching regions, indicating both increased water amount in the sub membrane and reorientation of molecules in the organic layer. The positive-going methylene stretching vibrational modes indicate tilting of carbohydrate chains with respect to surface normal, although their assignment to a particular component of anchoring or lipid layer is not accessible. Exposure to pH 7.3 solution red-shifted both methylene stretching modes by 2–3 cm^{-1} (cf. to as-formed tBLM in Figure 7) to 2854 and 2924 cm^{-1} , respectively.

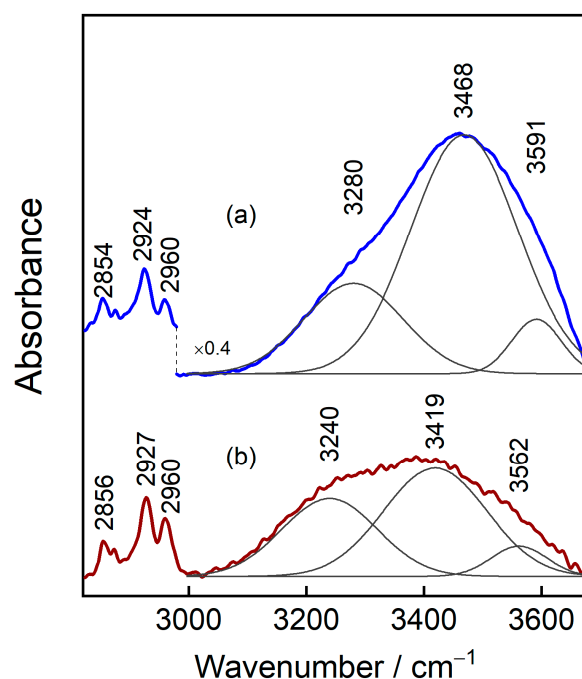


Figure 8. SEIRAS spectra of tBLM exposed to pH 7.3 (a) and then to 4.5 solutions (b). The reference spectrum was as-formed tBLM membrane in pH 4.5 phosphate solution.

A positive facing O–H stretching mode in Figure 8a indicates a surge of water content in the tBLM structure at pH = 7.3 compared to tBLMs exposed to a more acidic environment, pH = 4.4 (Figure 8b). The O–H spectral mode may be deconvoluted into three Gaussian–Lorentzian shape components. Two lower frequency components were previously defined as “network water” at 3250 and 3400 cm^{-1} , the former related to a solid-like network of strongly hydrogen-bonded water molecules and the latter (most intense component) to liquid state of water. The “multimer water” of water molecules forming a disturbed hydrogen-bond network may be associated with spectral component visible at 3600 cm^{-1} [53,54]. The positive intensity and shape of OH mode at pH 4.5 indicates that the system did not fully recover from structural rearrangements after exposure to pH 7.3. For more quantitative analysis, integral intensity ratios R_{network} and R_{multimer} are calculated and presented in Table 8. R_{network} indicates a population of strongly coupled water molecules, while R_{multimer} is related to a disturbed hydrogen-bond network [53]. For comparison, we have also measured bulk water placed on pristine silicon crystal in ATR mode (Table 8). In SEIRAS at pH 7.3, a surge of water to the sub membrane is detected, characterized by an increased portion of multimer and a rather small portion of network water compared to a bulk water ATR spectrum. Moreover, close analysis of peak positions revealed a noticeable upshift as high as 64 cm^{-1} , which points to decreasing H-bonding interaction among water molecules near the lipid membrane. Subsequent shifting back to pH 4.5 sharply decreased the water amount in the tBLM; however, there remained an

excess of it compared to the as-prepared tBLM. Thinning of lipid bilayer would explain positive bulk-like water mode; however, previous studies have found little to no dependence between pH and lipid layer thickness [20,21].

Table 8. Wavenumbers of O–H stretching modes and relative populations of network and multimer water.

No	pH	Wavenumber (cm ⁻¹)			$R_{network} = \frac{A_{3250}}{A_{3400}}$	$R_{multimer} = \frac{A_{3600}}{A_{3250} + A_{3400}}$
1	7.3	3280	3468	3591	0.35	0.08
2	4.5	3240	3419	3562	0.66	0.09
3	7.3	3276	3467	3593	0.43	0.08
4	4.5	3242	3414	3553	0.85	0.16
Si H ₂ O		3224	3404	3585	0.74	0.03

SEIRAS data suggest a considerable increase in water content in the sub membrane and/or bilayer region upon switching solution pH from 4.5 to 7.3. This supplemented water exhibits higher content of multimer fraction compared with network one. Such behavior might be related to the dominant contribution of the solvated ions. In other words, the shift of pH from 4.5 to 7.3 may be followed by an increase in the concentration of solvated ions in the sub membrane space, which will decrease the specific resistance of the sub membrane, and consequently, will translate into an upward shift of the admittance phase minimum, as observed by the EIS.

4. Conclusions

Due to their robust architecture and versatile configurations, there is increasing interest in tBLM-based biosensors [17]. Previous studies have demonstrated the versatility of tBLM systems using substrates coated with materials such as fluorine-doped tin oxide [55] and silver [56]; these tBLMs exhibit typical EIS features of lipid bilayer formation and pore-forming toxin activity. However, the choice of substrate material affects the quantitative features of the EIS response for reasons that are not fully understood. The construction of tBLM-based biosensors requires a strong fundamental understanding of how these systems behave in different aqueous environments. In this study, we re-evaluated the role of the sub-membrane region's contribution to the measured EIS of tBLMs. We show that for relatively high conducting defects (protein pores) with conductance above about 50 pS/defect, the measured impedance spectra, together with the defect density, are primarily determined by the submembrane resistivity. Any change in the resistivity of the sub-membrane is reflected in the spectral changes of the EIS, which are a priori indistinguishable from the changes in defect density. Therefore, the effects of pH variations on tBLMs were investigated in detail by EIS. We observed experimentally that the pH change from 4.4 to 7.1 triggered the increase of the admittance magnitude of tBLMs and the upshift of the admittance magnitude phase minimum towards higher frequencies. EIS experiments on these pristine tBLMs show an increase in the f_{min} position towards higher frequencies when the pH is changed from acidic to neutral. Notably, the pristine tBLMs with natural defects made from three different lipid compositions showed similar almost identical effects, unless the tBLMs contained charged lipids in their composition. The phase minimum shifts were consistently higher in the systems containing charged lipids, showing that the lipid composition, but not the defect type, is the dominant factor in determining pH-induced changes in the electrical properties of tBLMs.

The tBLMs reconstituted with two different types of pore-forming toxins, namely VLY (large pores) and MEL (small pores), responded to pH variation in a quantitatively similar way to membranes populated with natural defects. This suggests a dominant role for the submembrane (which is the same whether the tBLM contains natural or artificially introduced defects).

Finally, the SEIRA spectroscopy data explain that the main physical factor is responsible for the variation in submembrane resistivity. It was found that as the pH changes from acidic to neutral, the submembrane is flooded with a higher ion content, increasing the specific conductance and decreasing the specific resistance in the submembrane. The driving force for this is not entirely clear, but protonation of the lipid head groups and the resulting change in the charge balance of the confined space may be of primary importance.

The results of our study are important for the design of smart sensor systems to be used in environments with variable or unstable pH values. Since the readout signal of bio-sensing devices based on tBLMs is pH sensitive, this sensitivity needs to be taken into account if the devices are to be used in variable pH environments. Although the detection limit of tBLM-based biosensors is mainly determined by the specifics of the lipid bilayer and protein interactions, pH is one of the parameters that influence the magnitude of the response of tBLM-based biosensors. Therefore, the results obtained in the current study will help to understand the pH effect and thus improve the precision and consequently the detection limit of each analyte of interest.

EIS fitting analysis shows that the change in sub-membrane specific resistance $\Delta\rho_{sub}$ is similar for pristine and toxin-affected tBLMs analyzed under the conditions of hypotheses 2 and 3. This indicates that the observed pH-induced effect is due to a possible contribution of the submembrane region to the magnitude of the submembrane resistance, which in turn is translated into variations of the measured EIS. Surface-enhanced infrared absorption spectroscopy (SEIRAS), which allows us to directly probe the submembrane structure of tBLMs, suggests a significant increase in water content in the submembrane space and/or bilayer region upon changing pH from acidic to basic. We hypothesize that this increase in water content in the confined space between the electrode and the bilayer reflects an increase in the concentration of hydrated charge carriers, which may be related to an increase in the dielectric constant of the sub-membrane at elevated pH.

Supplementary Materials: The following supporting information can be downloaded at: <https://www.mdpi.com/article/10.3390/chemosensors11080450/s1>, Figure S1: Admittance Bode magnitude plots of pristine membrane corresponding to Figure 4; Figure S2: Admittance Bode magnitude plots of VLY affected membrane corresponding to Figure 5; Figure S3: Admittance Bode magnitude plots of MEL affected membrane corresponding to Figure 6; Figure S4: (A) EIS bode diagram of tBLM prepared from total lipid extract (TLE), pristine tBLM (solid line) and tBLM damaged by MEL (dashed line). Lines are fitted to the data obtained by assuming a negligible change in N_{def} and $P(N_{def})$. Orange color signifies pH 7.1; blue pH 4.4. (B) Defect density distribution functions obtained by fitting EIS spectra; Figure S5: (A) EIS bode diagram of tBLM prepared from TLE, pristine tBLM (solid line) and tBLM damaged by MEL (dashed line). Lines are fits to the data obtained by assuming negligible change in ρ_{sub} , ρ_{sub} values used in all calculations was $31,622 \Omega \text{ cm}^{-1}$. Orange color signifies pH 7.1; blue pH 4.4. (B) Defect density distribution functions obtained by fitting EIS spectra; Figure S6: (A) EIS bode diagram of tBLM prepared from TLE, pristine tBLM (solid line) and tBLM damaged by MEL (dashed line). Lines are fitted to the data obtained by assuming that average N_{def} does not change, while $P(N_{def})$ is allowed to vary, ρ_{sub} value used in all calculations was $31,622 \Omega \text{ cm}^{-1}$. Orange color signifies pH 7.1; blue pH 4.4. (B) Defect density distribution functions $P(N_{def})$ obtained by fitting EIS spectra.

Author Contributions: A.P.S.: Investigation, Data Curation, Formal analysis, Writing—original draft; F.A.: Investigation, Formal Analysis, Visualization; M.T.: Investigation, Formal analysis, Visualization; V.P.: Investigation, Formal analysis, Visualization; G.N.: Conceptualization, Resources, Writing—Review & editing. G.V.: Conceptualization, Resources, Writing—Review & editing. All authors have read and agreed to the published version of the manuscript.

Funding: This work was supported by Research Council of Lithuania, project number P-MIP-19-394 (QAPHOMEDA).

Institutional Review Board Statement: Not applicable.

Informed Consent Statement: Not applicable.

Data Availability Statement: Raw modelling data as well as the unprocessed experimental data are available from the authors on request. **Acknowledgement:** The authors thank Milda Plečkaitytė, from the Life Sciences Center at Vilnius University for purifying and providing vaginolysin used in the current study.

Conflicts of Interest: The authors declare no conflict of interest.

References

1. Agmon, E.; Stockwell, B.R. Lipid homeostasis and regulated cell death. *Curr. Opin. Chem. Biol.* **2017**, *39*, 83–89. [[CrossRef](#)] [[PubMed](#)]
2. Miyamoto, V.K.; Thompson, T.E. Some electrical properties of lipid bilayer membranes. *J. Colloid Interface Sci.* **1967**, *25*, 16–25. [[CrossRef](#)]
3. Penkauskas, T.; Preta, G. Biological applications of tethered bilayer lipid membranes. *Biochimie* **2019**, *157*, 131–141.
4. Raguse, B.; Braach-Maksvytis, V.; Cornell, B.A.; King, L.G.; Osman, P.D.; Pace, R.J.; Wieczorek, L. Tethered lipid bilayer membranes: Formation and ionic reservoir characterization. *Langmuir* **1998**, *14*, 648–659. [[CrossRef](#)]
5. Shenoy, S.; Moldovan, R.; Fitzpatrick, J.; Vanderah, D.J.; Deserno, M.; Lösche, M. In-plane homogeneity and lipid dynamics in tethered bilayer lipid membranes (tBLMs). *Soft Matter* **2010**, *6*, 1263–1274.
6. McGillivray, D.J.; Valincius, G.; Vanderah, D.J.; Febo-Ayala, W.; Woodward, J.T.; Heinrich, F.; Kasianowicz, J.J.; Lösche, M. Molecular-scale structural and functional characterization of sparsely tethered bilayer lipid membranes. *Biointerphases* **2007**, *2*, 21–33. [[CrossRef](#)]
7. Köper, I. Insulating tethered bilayer lipid membranes to study membrane proteins. *Mol. Biosyst.* **2007**, *3*, 651–657. [[CrossRef](#)]
8. Alghalayini, A.; Garcia, A.; Berry, T.; Cranfield, C.G. The use of tethered bilayer lipid membranes to identify the mechanisms of antimicrobial peptide interactions with lipid bilayers. *Antibiotics* **2019**, *8*, 12. [[CrossRef](#)]
9. Jadhav, S.R.; Sui, D.; Garavito, R.M.; Worden, R.M. Fabrication of highly insulating tethered bilayer lipid membrane using yeast cell membrane fractions for measuring ion channel activity. *J. Colloid Interface Sci.* **2008**, *322*, 465–472. [[CrossRef](#)] [[PubMed](#)]
10. Alobeedallah, H.; Cornell, B.; Coster, H. The effect of cholesterol on the voltage–current characteristics of tethered lipid membranes. *J. Membr. Biol.* **2020**, *253*, 319–330. [[CrossRef](#)]
11. Song, H.; Sinner, E.-K.; Knoll, W. Peptid-tethered bilayer lipid membranes and their interaction with Amyloid β -peptide. *Biointerphases* **2007**, *2*, 151–158. [[CrossRef](#)] [[PubMed](#)]
12. Guidelli, R.; Becucci, L. Functional activity of peptide ion channels in tethered bilayer lipid membranes. *Electrochem. Sci. Adv.* **2022**, *2*, e2100180.
13. Vockenroth, I.K.; Atanasova, P.P.; Jenkins, A.T.A.; Koeper, I. Incorporation of α -hemolysin in different tethered bilayer lipid membrane architectures. *Langmuir* **2008**, *24*, 496–502. [[CrossRef](#)]
14. Zieleniecki, J.L.; Nagarajan, Y.; Waters, S.; Rongala, J.; Thompson, V.; Hrmova, M.; Köper, I. Cell-free synthesis of a functional membrane transporter into a tethered bilayer lipid membrane. *Langmuir* **2016**, *32*, 2445–2449. [[CrossRef](#)] [[PubMed](#)]
15. Vockenroth, I.K.; Ohm, C.; Robertson, J.W.; McGillivray, D.J.; Lösche, M.; Köper, I. Stable insulating tethered bilayer lipid membranes. *Biointerphases* **2008**, *3*, FA68–FA73. [[CrossRef](#)] [[PubMed](#)]
16. Tun, T.N.; Jenkins, A.T.A. An electrochemical impedance study of the effect of pathogenic bacterial toxins on tethered bilayer lipid membrane. *Electrochem. Commun.* **2010**, *12*, 1411–1415. [[CrossRef](#)]
17. Zhou, W.; Burke, P.J. Versatile Bottom-Up Synthesis of Tethered Bilayer Lipid Membranes on Nanoelectronic Biosensor Devices. *ACS Appl. Mater. Interfaces* **2017**, *9*, 14618–14632. [[CrossRef](#)] [[PubMed](#)]
18. Krishna, G.; Schulte, J.; Cornell, B.A.; Pace, R.J.; Osman, P.D. Tethered bilayer membranes containing ionic reservoirs: Selectivity and conductance. *Langmuir* **2003**, *19*, 2294–2305. [[CrossRef](#)]
19. Valincius, G.; Meškauskas, T.; Ivanauskas, F. Electrochemical impedance spectroscopy of tethered bilayer membranes. *Langmuir* **2012**, *28*, 977–990. [[CrossRef](#)]
20. Cranfield, C.G.; Berry, T.; Holt, S.A.; Hossain, K.R.; Le Brun, A.P.; Carne, S.; Al Khamici, H.; Coster, H.; Valenzuela, S.M.; Cornell, B. Evidence of the Key Role of H(3)O(+) in Phospholipid Membrane Morphology. *Langmuir* **2016**, *32*, 10725–10734. [[CrossRef](#)] [[PubMed](#)]
21. Silin, V.I.; Hoogerheide, D.P. pH dependent electrical properties of the inner- and outer-leaflets of biomimetic cell membranes. *J. Colloid Interface Sci.* **2021**, *594*, 279–289. [[CrossRef](#)]
22. Santos, H.A.; Vila-Viçosa, D.; Teixeira, V.H.; Baptista, A.M.; Machuqueiro, M. Constant-pH MD simulations of DMPA/DMPC lipid bilayers. *J. Chem. Theory Comput.* **2015**, *11*, 5973–5979. [[CrossRef](#)] [[PubMed](#)]
23. Van Den Bogaart, G.; Guzmán, J.V.; Mika, J.T.; Poolman, B. On the mechanism of pore formation by melittin. *J. Biol. Chem.* **2008**, *283*, 33854–33857. [[CrossRef](#)]
24. Sabapathy, T.; Deplazes, E.; Mancera, R.L. Revisiting the interaction of melittin with phospholipid bilayers: The effects of concentration and ionic strength. *Int. J. Mol. Sci.* **2020**, *21*, 746. [[CrossRef](#)] [[PubMed](#)]
25. Terwilliger, C.; Eisenberg, D. The structure of melittin. *J. Biol. Chem.* **1982**, *257*, 6–016. [[CrossRef](#)]
26. Ambrulevicius, F.; Valincius, G. Electrochemical impedance spectrum reveals structural details of distribution of pores and defects in supported phospholipid bilayers. *Bioelectrochemistry* **2022**, *146*, 108092. [[CrossRef](#)]

27. Zvirbliene, A.; Pleckaityte, M.; Lasickiene, R.; Kucinskaite-Kodze, I.; Zvirblis, G. Production and characterization of monoclonal antibodies against vaginolysin: Mapping of a region critical for its cytolytic activity. *Toxicon* **2010**, *56*, 19–28. [[CrossRef](#)] [[PubMed](#)]
28. Raila, T.; Penkauskas, T.; Ambrulevičius, F.; Jankunec, M.; Meškauskas, T.; Valinčius, G. AI-based atomic force microscopy image analysis allows to predict electrochemical impedance spectra of defects in tethered bilayer membranes. *Sci. Rep.* **2022**, *12*, 1127. [[CrossRef](#)] [[PubMed](#)]
29. Raila, T.; Ambrulevičius, F.; Penkauskas, T.; Jankunec, M.; Meškauskas, T.; Vanderah, D.J.; Valincius, G. Clusters of protein pores in phospholipid bilayer membranes can be identified and characterized by electrochemical impedance spectroscopy. *Electrochim. Acta* **2020**, *364*, 137179. [[CrossRef](#)]
30. Yaguchi, M.; Uchida, T.; Motobayashi, K.; Osawa, M. Speciation of adsorbed phosphate at gold electrodes: A combined surface-enhanced infrared absorption spectroscopy and DFT study. *J. Phys. Chem. Lett.* **2016**, *7*, 3097–3102. [[CrossRef](#)]
31. Ma, J.; Li, K.; Li, Z.; Qiu, Y.; Si, W.; Ge, Y.; Sha, J.; Liu, L.; Xie, X.; Yi, H. Drastically reduced ion mobility in a nanopore due to enhanced pairing and collisions between dehydrated ions. *J. Am. Chem. Soc.* **2019**, *141*, 4264–4272. [[CrossRef](#)] [[PubMed](#)]
32. Chakraborty, S.; Molugu, T.R.; Doktorova, M.; Heberle, F.A.; Scott, H.L.; Kelley, E.G.; Nagao, M.; Dzikovski, B.G.; Standaert, R.F.; Barrera, F.N. Stiffening of Phosphocholine Membranes by Cholesterol. *Biophys. J.* **2020**, *118*, 86a. [[CrossRef](#)]
33. Chakraborty, S.; Doktorova, M.; Molugu, T.R.; Heberle, F.A.; Scott, H.L.; Dzikovski, B.; Nagao, M.; Stingaciu, L.-R.; Standaert, R.F.; Barrera, F.N. How cholesterol stiffens unsaturated lipid membranes. *Proc. Natl. Acad. Sci. USA* **2020**, *117*, 21896–21905. [[CrossRef](#)]
34. Reddy, A.S.; Warshaviak, D.T.; Chachisvilis, M. Effect of membrane tension on the physical properties of DOPC lipid bilayer membrane. *Biochim. Biophys. Acta (BBA)—Biomembr.* **2012**, *1818*, 2271–2281. [[CrossRef](#)]
35. Rojko, N.; Anderluh, G. How lipid membranes affect pore forming toxin activity. *Acc. Chem. Res.* **2015**, *48*, 3073–3079. [[CrossRef](#)]
36. Gilbert, R.J. Cholesterol-dependent cytolysins. In *Proteins Membrane Binding and Pore Formation*; Springer: New York, NY, USA, 2010; pp. 56–66.
37. Lee, M.-T.; Sun, T.-L.; Hung, W.-C.; Huang, H.W. Process of inducing pores in membranes by melittin. *Proc. Natl. Acad. Sci. USA* **2013**, *110*, 14243–14248. [[CrossRef](#)]
38. Sabirovas, T.; Valiūnienė, A.; Valincius, G. Hybrid bilayer membranes on metallurgical polished aluminum. *Sci. Rep.* **2021**, *11*, 9648. [[CrossRef](#)]
39. Wessman, P.; Strömstedt, A.A.; Malmsten, M.; Edwards, K. Melittin-lipid bilayer interactions and the role of cholesterol. *Biophys. J.* **2008**, *95*, 4324–4336. [[CrossRef](#)] [[PubMed](#)]
40. Qian, S.; Heller, W.T. Melittin-induced cholesterol reorganization in lipid bilayer membranes. *Biochim. Biophys. Acta (BBA)—Biomembr.* **2015**, *1848*, 2253–2260. [[CrossRef](#)] [[PubMed](#)]
41. Deng, Z.; Lu, X.; Xu, C.; Yuan, B.; Yang, K. Lipid-specific interactions determine the organization and dynamics of membrane-active peptide melittin. *Soft Matter* **2020**, *16*, 3498–3504. [[CrossRef](#)] [[PubMed](#)]
42. Lowe, L.A.; Kindt, J.T.; Cranfield, C.; Cornell, B.; Macmillan, A.; Wang, A. Subtle changes in pH affect the packing and robustness of fatty acid bilayers. *Soft Matter* **2022**, *18*, 3498–3504. [[CrossRef](#)]
43. Ad, P.; Figaszewski, Z. Effect of pH on interfacial tension of bilayer lipid membrane. *Biophys. J.* **2000**, *78*, 812–817.
44. Aroti, A.; Leontidis, E.; Dubois, M.; Zemb, T. Effects of monovalent anions of the Hofmeister series on DPPC lipid bilayers Part I: Swelling and in-plane equations of state. *Biophys. J.* **2007**, *93*, 1580–1590.
45. Wu, X.; Wang, P.; Lewis, W.; Jiang, Y.-B.; Gale, P.A. Measuring anion binding at biomembrane interfaces. *Nat. Commun.* **2022**, *13*, 4623. [[CrossRef](#)]
46. Redondo-Morata, L.; Giannotti, M.I.; Sanz, F. Structural impact of cations on lipid bilayer models: Nanomechanical properties by AFM-force spectroscopy. *Mol. Membr. Biol.* **2014**, *31*, 17–28. [[CrossRef](#)] [[PubMed](#)]
47. Yang, X.; Sun, Z.; Low, T.; Hu, H.; Guo, X.; de Abajo, F.J.G.; Avouris, P.; Dai, Q. Nanomaterial-based plasmon-enhanced infrared spectroscopy. *Adv. Mater.* **2018**, *30*, 1704896.
48. Li, J.; Zheng, B.; Zhang, Q.-W.; Liu, Y.; Shi, C.-F.; Wang, F.-B.; Wang, K.; Xia, X.-H. Attenuated total reflection surface-enhanced infrared absorption spectroscopy: A powerful technique for bioanalysis. *J. Anal. Test.* **2017**, *1*, 8. [[CrossRef](#)]
49. Ataka, K.; Drauschke, J.; Stulberg, V.; Koksche, B.; Heberle, J. pH-induced insertion of pHLIP into a lipid bilayer: In-situ SEIRAS characterization of a folding intermediate at neutral pH. *Biochim. Biophys. Acta (BBA)—Biomembr.* **2022**, *1864*, 183873. [[CrossRef](#)] [[PubMed](#)]
50. Forbrig, E.; Staffa, J.K.; Salewski, J.; Mroginski, M.A.; Hildebrandt, P.; Kozuch, J. Monitoring the orientational changes of alamethicin during incorporation into bilayer lipid membranes. *Langmuir* **2018**, *34*, 2373–2385. [[CrossRef](#)] [[PubMed](#)]
51. Dziubak, D.; Sek, S. Physicochemical Characterization of Sparsely Tethered Bilayer Lipid Membranes: Structure of Submembrane Water and Nanomechanical Properties. *ChemElectroChem* **2021**, *8*, 2564–2571. [[CrossRef](#)]
52. Uchida, T.; Osawa, M.; Lipkowski, J. SEIRAS studies of water structure at the gold electrode surface in the presence of supported lipid bilayer. *J. Electroanal. Chem.* **2014**, *716*, 112–119. [[CrossRef](#)]
53. Su, Z.; Juhaniwicz-Debinska, J.; Sek, S.; Lipkowski, J. Water structure in the submembrane region of a floating lipid bilayer: The effect of an ion channel formation and the channel blocker. *Langmuir* **2019**, *36*, 409–418. [[CrossRef](#)] [[PubMed](#)]
54. Disalvo, E.A.; Frias, M. Water state and carbonyl distribution populations in confined regions of lipid bilayers observed by FTIR spectroscopy. *Langmuir* **2013**, *29*, 6969–6974. [[CrossRef](#)] [[PubMed](#)]

55. Gabriunaite, I.; Valiūnienė, A.; Valincius, G. Formation and properties of phospholipid bilayers on fluorine doped tin oxide electrodes. *Electrochim. Acta* **2018**, *283*, 1351–1358. [[CrossRef](#)]
56. Aleknavičienė, I.; Jankunec, M.; Penkauskas, T.; Valincius, G. Electrochemical properties of tethered lipid bilayers on thin film silver substrates. *Electrochim. Acta* **2021**, *389*, 138726. [[CrossRef](#)]

Disclaimer/Publisher’s Note: The statements, opinions and data contained in all publications are solely those of the individual author(s) and contributor(s) and not of MDPI and/or the editor(s). MDPI and/or the editor(s) disclaim responsibility for any injury to people or property resulting from any ideas, methods, instructions or products referred to in the content.